Isolated core excitation of ^{11}BH: Photoabsorption in competition with Rydberg predissociation

C. Ricardo Viteri and Andrew T. Gilkison*
Department of Chemistry, Purdue University, West Lafayette, Indiana 47907, USA

Scott J. Rixon and Edward R. Grant†
Department of Chemistry, University of British Columbia, Vancouver, British Columbia, Canada V6 T 1Z3
(Received 21 August 2006; published 11 January 2007)

The ionization-detected multiresonant absorption spectrum of the high Rydberg states of ^{11}BH shows evidence of a valence electronic excitation of the $X\,^2\Sigma^+$ $^{11}BH^+$ core in which the principal and azimuthal quantum numbers of a bound Rydberg electron are conserved. This phenomenon, known as isolated core excitation (ICE), has been previously reported with Rydberg quantum state specificity only for atoms. In the present triple-resonant photoexcitation experiment, the third laser frequency happens to scan an energy interval of coincidental fourth-photon resonance with transitions in the $A\,^2\Pi$-$X\,^2\Sigma^+$ system of the $^{11}BH^+$ ion core. For a certain range of principal quantum number n, we find that the initially prepared Rydberg electron remains unaffected while the core undergoes an adventitious, strongly allowed valence electron transition, taking the system from a Rydberg level that converges to the $X\,^2\Sigma^+$ state of $^{11}BH^+$ to a corresponding level converging to excited $^{11}BH^+$ $A\,^2\Pi$. We denote this absorption as $|A\,^2\Pi\rangle|nl\rangle \leftarrow |X\,^2\Sigma^+\rangle|nl\rangle$. Using a simple mathematical model for which only transitions vertical in n and l are allowed, we show that the interval of principal quantum number over which the rate of adventitious ICE exceeds that of $^{11}BH^*$ dissociation depends on the finite linewidths and positions of $|A\,^2\Pi\rangle|nl\rangle$ features and on the n-dependent predissociative lifetimes of $^{11}BH^*$ Rydberg molecules.

DOI: 10.1103/PhysRevA.75.013410 PACS number(s): 33.80.Rv, 33.40.+f, 33.80.Eh, 33.80.Wz

I. INTRODUCTION

Nearly 30 years have passed since Cooke and co-workers introduced isolated core excitation (ICE) as a method to spectroscopically characterize doubly excited states in Group II atoms [1]. ICE relies for its effectiveness on the approximate separability of electrons in valence and Rydberg orbitals. A high-n Rydberg orbital, with electron density extending to the classical turning point region, can be expected to overlap negligibly with the wave function of a tightly bound valence electron. This isolated core picture implies that the central atomic ion can be treated as if it is independent of the orbiting Rydberg electron [2,3]. The energy-dependent cross section for ICE to a final autoionizing state depends then only on the oscillator strength for ionic photoexcitation, the density and linewidths of final autoionizing states, and a center frequency shift determined by the difference between quantum defects of the initial and final states. Since isolated core excitation prepares doubly excited states by strongly allowed single-electron excitation, ICE spectra do not suffer from interference owing to the simultaneous excitation of multiple weakly allowed transitions. ICE scans therefore offer a straightforward means of extracting quantum defects and autoionization lifetimes [4]. The photoabsorption cross section near a resonance is often a simple Lorentzian [5]. Consequently, this method has been used extensively to study the spectroscopy of doubly excited states. ICE experiments have characterized great number of autoionizing series in Ba, Sr, Ca, and Mg [2–9].

In molecules, Rydberg electrons have been exploited as a spectroscopic tool to map the excited states of cations in a variety of applications [10]. Several named methods make use of the distinct character of molecular Rydberg states [11]. Zero electron kinetic energy (ZEKE) spectroscopy [12,13] precisely registers state-specified ionization limits by the pulsed field ionization of long-lived molecular Rydberg states ($n>100$) [14]. Mass-analyzed threshold ionization (MATI) spectroscopy [11,15], makes similar use of near-threshold molecular Rydberg states, but ultimately detects ions rather than electrons.

The possibility of core exciting a Rydberg molecule was first recognized by Johnson and co-workers [16], who developed a technique known as photoinduced Rydberg ionization (PIRI). This technique has proven useful as a means for obtaining high-resolution vibrational and electronic spectra of mass-resolved cations [17]. Instead of field ionizing the Rydberg molecules (as in ZEKE or MATI), core electronic or vibrational transitions are photoexcited. The core-excited Rydberg molecules autoionize to produce a detectable ion signal. Monitoring the photoinduced autoionization signal while scanning the core-excitation photon energy yields a spectrum of the excited ionic state of interest [18]. This method relies both on the long lifetime of high Rydberg molecules, and on a negligible, but as yet uncharacterized interaction of the Rydberg electrons with optical radiation [17].

Before the development of PIRI, Kong *et al.*, using pulsed field ionization threshold photoelectron spectroscopy (PFI-ZEKE) to study the $A\,^2\Sigma^+$ state of N_2O^+ [19], showed that an ion core can radiatively relax without losing a bound high-n Rydberg electron. However, neither the PIRI nor the core

*Present address: Schering-Plough, 2000 Galloping Hill Road, Kenilworth, NJ 07033-0530.
†Author to whom correspondence should be addressed. Electronic address: edgrant@chem.ubc.ca

emission experiment speaks to any change in state of the Rydberg electron associated with excitation or dexcitation of the core.

The present work reports a complete molecular analog of ICE as observed for atoms, in which a high-n molecular Rydberg electron maintains the role of a spectator. Our experiment uses a two-color (ω_1 plus ω_2) double-resonant laser excitation scheme to promote ^{11}BH radicals to a specific rovibrational level ($B\ ^1\Sigma^+$, $\nu'=0$, $N'=0$). From this gateway level, we scan a third color (ω_3) laser to populate Rydberg states in series that converge to the ground vibrational level of the $X\ ^2\Sigma^+$ state of $^{11}BH^+$, which we denote by $|X\ ^2\Sigma^+\rangle|nl\rangle$. These series are confined by angular momentum selection rules to converge to the $N^+=0$, 1, and 2 core rotational levels. Depending on n, this scan interval allows adventitious $|A\ ^2\Pi, \nu^+=0\rangle|nl\rangle \leftarrow |X\ ^2\Sigma^+, \nu^+=0\rangle|nl\rangle$ isolated core excitation (ICE) to occur by absorption of a second ω_3 photon before the $|X\ ^2\Sigma^+, \nu^+=0\rangle|nl\rangle$ $^{11}BH^*$ state can predissociate. Using a simple mathematical model for which only transitions vertical in n and l are allowed, we show that the interval of n for which the $|A\ ^2\Pi\rangle|nl\rangle \leftarrow |X\ ^2\Sigma^+\rangle|nl\rangle$ ICE rate exceeds that of the dissociation of $|X\ ^2\Sigma^+\rangle|nl\rangle$ $^{11}BH^*$ depends on the finite linewidths and positions of the $|A\ ^2\Pi\rangle|nl\rangle$ features and on the n-dependent predissociative lifetimes of $^{11}BH^*$ Rydberg molecules.

II. EXPERIMENT

A free jet expansion containing a mixture of 5% B_2H_6 (synthesized as per Jeffers [20]) in H_2 maintained at 3.0 atm is released from a pulsed solenoid nozzle (10 Hz, General Valve, IOTA-1) into a turbomolecular pumped vacuum chamber at a background pressure of about 10^{-6} Torr. An ArF excimer laser ($\lambda=193$ nm, Lambda Physik, Compex 201) focused near the nozzle exit photolyzes this mixture, producing rotationally cooled BH radicals (80.1% ^{11}BH, 19.9% ^{10}BH); these propagate 10 cm downstream to a laser photoionization time-of-flight mass spectrometer (R.M. Jordan Co., 1 m Wiley-McLaren TOF-MS). Here, three pulsed collimated lasers coincide to sequentially excite ^{11}BH molecules, as depicted in Fig. 1.

In the first step (ω_1), a Nd:YAG pumped OPO ($\lambda=480.1$ nm, Continuum Precision 8000 Series/Continuum Panther) transfers ^{11}BH population from the $X\ ^1\Sigma^+$, $\nu''=1$, $N''=0$ level to $A\ ^1\Pi$, $\nu'=0$, $N'=1$; the large ^{11}B-^{10}B vibrational isotopic shift of the A-X (0,1) band precludes excitation of ^{10}BH. A second laser (ω_2), the BBO-doubled output of a XeCl excimer pumped dye laser ($\lambda=341.9$ nm, Lambda Physik EMG 201/FL 3002) promotes the $A\ ^1\Pi$ state population to the $B\ ^1\Sigma^+$, $\nu'=0$, $N'=0$ rovibrational level, which serves as a gateway state for transitions to high Rydberg states driven by a companion dye laser (Lambda Physik FL 2001) pumped by the same EMG 201. This laser (ω_3) reaches $|X\ ^2\Sigma^+, \nu^+=0\rangle|nl\rangle$ Rydberg states of ^{11}BH that form series over the interval within 1000 cm^{-1} of the adiabatic ionization threshold. A home-built delay generator synchronizes the photolysis and various pump laser pulses to maximize this process. A fraction of the $^{11}BH^*$ molecules so prepared are detected as ions after having followed one of two photo-paths driven by the still-present laser fields of ω_2 or ω_3, as shown in Fig. 2.

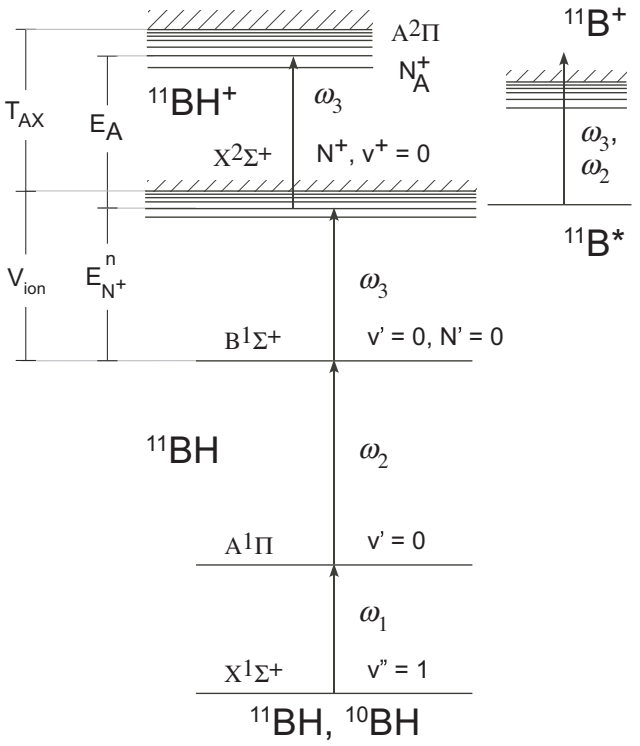

FIG. 1. Energy-level diagram showing the pulse sequence (ω_1 and ω_2) by which vibrationally excited ^{11}BH molecules are promoted first to a selected rovibrational level of the $A\ ^1\Pi$ valence state, then to the gateway $B\ ^1\Sigma^+$, $\nu'=0$, $N'=0$ Rydberg state. A third counter-propagating laser, ω_3, accesses the $|X\ ^2\Sigma^+, \nu^+=0, N^+\rangle|nl\rangle$ Rydberg states with $N^+=0$, 1 or 2; these have energy E^n_{N+} and rotational ionization thresholds $V_{\rm ion}(N^+)$. Such a state can follow one of two paths. It can dissociate to form $^{11}B^*$, which ionizes following one-photon absorption in the still-present ω_2 and ω_3 laser fields. Alternatively, when laser frequency ω_3 coincides with a transition energy $T_{AX}(N^+, N_A^+)$ of the $A^2\Pi$-$X\ ^2\Sigma^+$ (0,0) band of $^{11}BH^+$, the Rydberg state $|X\ ^2\Sigma^+, \nu^+=0, N^+\rangle|nl\rangle$ can absorb a photon. In the simplest form of this interaction, the initially prepared high-Rydberg electron acts as a spectator to an allowed $A\ ^2\Pi \leftarrow X\ ^2\Sigma^+$ valence electronic transition in the ion core, which occurs with an on-resonance energy $E_A(n, N^+, N_A^+)$ detuned from $E^n_{N^+}$ by a small amount as per Eq. (6).

A coincidental near-resonance between various particular tunings of the ω_3 laser and the $A\ ^2\Pi$-$X\ ^2\Sigma^+$ (0,0) band of

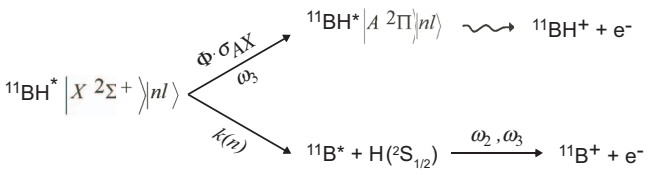

FIG. 2. Competition between light absorption and neutral fragmentation in Rydberg states of ^{11}BH. The interval of n for which the rate of photoabsorption, $\Phi\sigma_{AX}$, exceeds the predissociation rate, $k(n)$, depends on the finite linewidths and positions of $|A\ ^2\Pi\rangle|nl\rangle$ Rydberg features.

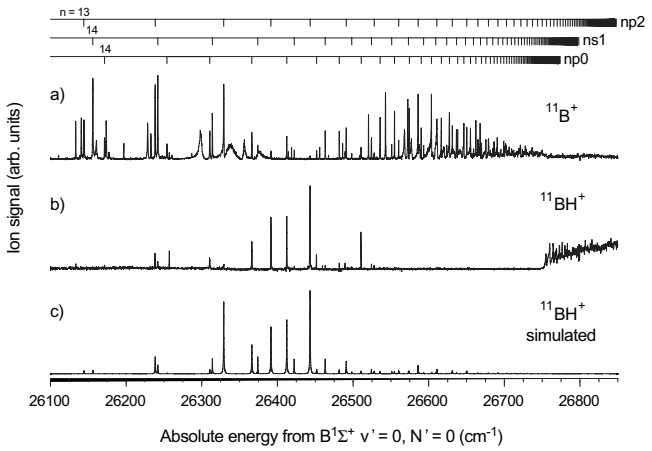

FIG. 3. Ionization-detected absorption structure observed at (a) 11 amu ($^{11}B^+$) and (b) 12 amu ($^{11}BH^+$) for transitions originating from the $B\ ^1\Sigma^+$, $\nu'=0$, $N'=0$ state of ^{11}BH converging to thresholds associated with the $X\ ^2\Sigma^+\nu^+=0$ state of $^{11}BH^+$. Ladders labeled by principal quantum numbers mark Rydberg resonances converging to rotational states $N^+=0$, 1 and 2. The ion signal detected at 12 amu shows the distribution of $^{11}BH^+$ features centered around $n=17-18$ as core $A\ ^2\Pi \leftarrow X\ ^2\Sigma^+$ transitions. The simulated spectrum in trace (c) is based on a mathematical model where the isolated-core excitations are vertical in principal quantum number n and orbital angular momentum l.

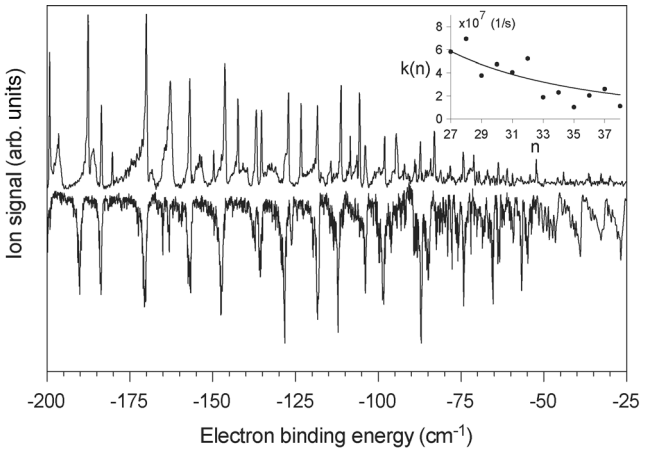

FIG. 4. Comparison of line shapes and intensities distributions of predissociating Rydberg series converging to $\nu^+=0$ (top, present work) with autoionizing Rydberg series converging to $\nu^+=1$ (bottom, from Ref. [24]). Only $^{11}BH^*$ Rydberg molecules which dissociate during the 10 ns that the laser fields persist are resonantly detected in the $^{11}B^+$ mass channel. In the region of high-n Rydberg states ($n=27-38$), the intensities of resonances detected through the dissociation channel decreases systematically with increasing principal quantum number. Taking these relative intensities, we use Eq. (2) to estimate predissociation constants $k(n)$ as plotted in the inset. The solid curve is obtained by fitting these 12 data points to Eq. (3).

$^{11}BH^+$ [21,22] can electronically excite the ion core in the presence of a spectator Rydberg electron (ICE). Afterward, electronic autoionization of the core-excited molecule yields $^{11}BH^+$. Alternatively, the high-Rydberg molecule can spontaneously dissociate into $^{11}B^*$ and H, and either of the ω_2 or ω_3 lasers has sufficient photon energy to ionize the excited boron atom product.

The 11 and 12 amu channels of the TOF-MS monitor, respectively, the dissociation ($^{11}B^+$) and ICE ($^{11}BH^+$) ion signals. The region between the repeller and extractor grids is held at zero potential during each laser excitation sequence. A pulsed 400 V/cm field applied 50 ns later directs ions into the flight region of a TOF-MS, where they are detected by a two-stage microchannel plate detector. As the ω_3 laser scans, the $\times 10$ preamplified ion signal is averaged by a digital oscilloscope (LeCroy 9400, 125 MHz) and recorded using LabVIEW data acquisition software. The dye laser wavelengths are calibrated with optogalvanic lines from a Fischer Scientific Fe/Ne hollow cathode lamp, standardized to measurements reported by Ashworth and Brown [23].

III. RESULTS

In two previous presentations on ^{11}BH, we have reported the vibrational autoionization spectrum of $|X\ ^2\Sigma^+\rangle|nl\rangle$ Rydberg resonances with core levels $\nu^+=1-4$, and a predissociation spectrum of vibrationless $|X\ ^2\Sigma^+, \nu^+=0\rangle|nl\rangle$ resonances [24,25]. In this earlier work, we assigned Rydberg series converging to the $N^+=0$, 1, and 2 rotational limits of these five vibrational levels based on angular momentum selection rules and on phenomenological quantum defects determined by line positions. The ion signal observed at mass 11 in the present work, shown in Fig. 3(a), contains predissociating Rydberg resonances that converge to these N^+ limits for $X\ ^2\Sigma^+$, $\nu^+=0$. These features have asymmetric Fano profiles, as previously found in the autoionization spectra of the $\nu^+=1$, 2, and 3 Rydberg series. Figure 4 shows, for example, a comparison to our previous data for $\nu^+=1$ [24,25]. These profiles signal strong coupling with a neutral continuum that has a large transition moment for direct absorption.

Following arguments presented previously [26], the discrete features in this trace must represent predissociation of $|X\ ^2\Sigma^+, \nu^+=0\rangle|nl\rangle$ $^{11}BH^*$ molecules followed by photoionization of nascent electronically excited $^{11}B^*$ atoms. Such a mechanism is reasonable because the pulse widths of the ω_2 and ω_3 lasers compare with the 4–20 ns radiative lifetimes measured for various $1s^22s^2ns$ and $1s^22s^2nd$ $^{11}B^*$ states [27]. Moreover, the photon energies of these lasers are sufficient to photoionize boron from any of these states, but not from the ground state [28,29]. All of these facts explain both the presence of discrete $^{11}BH^*$ Rydberg features and the absence of a continuous background from the ionization of ground state B atoms created originally in the excimer-laser photolysis of B_2H_6.

The spectrum in Fig. 3(b), recorded at the $^{11}BH^+$ mass, should show no signal below the lowest ionization threshold at $X\ ^2\Sigma^+$, $\nu^+=0$, $N^+=0$. However, in the region extending about 20 cm^{-1} below this limit, we observe an autoionization spectrum, the dominant features of which converge to $N^+=2$. These appear as a result of rotational coupling between $N^+=0$ states, which form an effective continuum for $n \geqslant 78$ by pulsed field ionization, and the $N^+=2$ series ($n=35-41$), a phenomenon previously observed in our laboratory in ZEKE experiments on NO_2 [30].

TABLE I. Transition energies, $T_{AX}(N^+,N_A^+)$, in cm^{-1}, of the nine pathways for the $A\ ^2\Pi \leftarrow X\ ^2\Sigma^+$ valence electronic ion core excitation as shown in Fig. 5 (from Ref. [22]).

	$A\ ^2\Pi_{1/2}$			$A\ ^2\Pi_{3/2}$	
N^+	1	2	3	2	3
0	26390.1				
1	26365.3	26410.7		26406.5	
2	26315.8	26361.1	26430.1	26356.9	26427.3

More significantly, we find another set of lines in the $^{11}BH^+$ spectrum at lower energy in the ω_3 interval from 26 100 to 26 550 cm^{-1}. These lines also appear in the $^{11}B^+$ spectrum, where they can be readily assigned to $|X\ ^2\Sigma^+, \nu^+=0\rangle|nl\rangle$ Rydberg series for $N^+=0$, 1 and 2. For the *np* series converging to $N^+=0$ and 2, features appear in the $^{11}BH^+$ spectrum with $n=14-23$ and 13–19, respectively. Several other exceedingly weak features with $n=14-21$ can be assigned as members of the *ns* series converging to $N^+=1$.

As indicated in Table I, the low-N lines of the $A\ ^2\Pi$ -$X\ ^2\Sigma^+$ (0,0) band of $^{11}BH^+$ fall at transition energies nearly equal to the third-photon frequencies of these Rydberg features [22]. Thus, over a short interval of the third-photon spectrum, we promote molecules to certain particular $|X\ ^2\Sigma^+, \nu^+=0\rangle|nl\rangle$ Rydberg states by ω_3 fields that happen to resonate as well with electronic transitions in the core to accessible rotational levels of the $^{11}BH^+$ valence excited $A\ ^2\Pi$, $\nu^+=0$ state. If the $|nl\rangle$ Rydberg state conserves n and l, in other words, if the Rydberg electron acts as a spectator, such adventitious core excitation transitions will occur only at ω_3 wave numbers that meet the double resonance condition for excitation from $(3s)\ B\ ^1\Sigma^+$, $\nu'=0$, $N'=0$ to $|X\ ^2\Sigma^+, \nu^+=0\rangle|nl\rangle$ and, in the core, from $X\ ^2\Sigma^+$, $\nu^+=0$, N^+ to $A\ ^2\Pi$, $\nu^+=0$, N^+ or $N^+\pm1$. Once formed, such core-excited $|A\ ^2\Pi\rangle|nl\rangle$ Rydberg states can be expected to readily form $^{11}BH^+$ by electronic autoionization.

It can be noted from Fig. 3 that for the most part Rydberg features of $|X\ ^2\Sigma^+, \nu^+=0\rangle|nl\rangle$ $^{11}BH^*$ common to the mass 11 and mass 12 spectra, generated, respectively, by predissociation and by isolated core excitation (ICE), have complementary intensities. It is therefore reasonable to regard these relative intensities as a measure of the competition between these two processes. We have considered this competition more quantitatively to generate the simulation of the mass 12 signal shown in Fig. 3(c).

IV. DISCUSSION

To model intensities in the spectrum of discrete $^{11}BH^+$ features that appear as a consequence of isolated core excitation, we must first consider the relative number of ^{11}BH molecules that remain excited to $|X\ ^2\Sigma^+, \nu^+=0\rangle|nl\rangle$ Rydberg states during the interval of time that the sample is illuminated by ω_3. We know that some fraction of these excited states must dissociate during this time to produce the excited boron atoms that then absorb another photon from the ω_3 field to form the $^{11}B^+$ signal that carries the spectrum of Rydberg series converging to the vibrational ground state of the cation. Obviously some must also survive for a time sufficient to undergo a core excitation on resonance leading to the formation of $^{11}BH^+$.

If the predissociation of high-Rydberg $^{11}BH^*$ proceeds according to

$$^{11}BH|X\ ^2\Sigma^+, \nu^+=0, N^+\rangle|nl\rangle \rightarrow {}^{11}B^* + H(^2S)$$

with rate constant, $k(n)$, the rate of $^{11}BH^*$ loss is

$$-\frac{d[^{11}BH^*]}{dt} = k(n)[^{11}BH^*] \tag{1}$$

and the fraction of $^{11}BH^*$ molecules that remain at the end of the $t=10$ ns laser pulses of ω_2 and ω_3 can be written as

$$\frac{[^{11}BH^*]_t}{[^{11}BH^*]_0} = 1 - \exp[-k(n)t]. \tag{2}$$

Assuming that $[^{11}BH^*]_0$, the initial density of $|X\ ^2\Sigma^+, \nu^+=0, N^+=0\rangle|nl\rangle$ Rydberg states is the same for each resonance, we can use the signal intensity observed for the last 12 assignable lines in the $^{11}B^+$ spectrum ($n=27-38$) to estimate values for $k(n)$. As can be seen in Fig. 4, by $n=38$ these intensities fall to about one-tenth the relatively constant magnitude of features in the spectrum at lower n. We arbitrarily assign a rate constant, $k(n)\approx 1\times10^7\ s^{-1}$ for predissociation at $n=38$, which corresponds to a predisociative lifetime 10 times longer than the ω_3 pulse duration. From this point of reference, we adopt a common convention for molecular Rydberg states and extrapolate to lower values of n according to

$$k(n) = k_r/n^3, \tag{3}$$

where k_r is a reduced rate constant chosen to give $k(n)=1\times10^7\ s^{-1}$ for $n=38$. A curve plotted in Fig. 4 shows how this extrapolation conforms with trends in the relative yield of $^{11}B^*$ predissociation product available to photoionize, as reflected by the $^{11}B^+$ signal intensities. We have extrapolated this curve further to estimate predissociation constants for the lower $^{11}BH^*$ Rydberg states for which ICE is observed. These estimates are listed in Table II.

Features that appear in both the $^{11}BH^+$ and $^{11}B^+$ mass channels originate from Rydberg states of ^{11}BH insufficiently energetic to ionize spontaneously. Absorption at ω_2 or ω_3 by a high-n Rydberg electron below the $\nu^+=0$ ionization threshold is unlikely because such transitions extend far into the continuum where ejected electron velocities are high and corresponding absorption cross sections are low. However, as

TABLE II. Numerical values of various parameters used to generate the simulated $^{11}BH^+$ spectrum shown in Fig. 3(c). Predissociation constants $k(n)$ are estimated using Eq. (3), photoabsorption rates $\Phi\sigma_{AX}(\Delta)$ from Eqs. (7) and (8) [Δ is obtained from Eq. (6)], and $|A\ ^2\Pi\rangle|nl\rangle$ linewidths from Eq. (5). Energies $E^n_{N^+}$ of transitions from $B\ ^1\Sigma^+\ \nu'=0$, $N'=0$ to the various $|X\ ^2\Sigma^+,\nu^+=0\rangle|nl\rangle$ Rydberg levels are measured from the spectra. These converge to rotational states $N^+=0$, 1, and 2 at 26 773.6, 26 798.4, and 26 847.84 cm^{-1} respectively. Energy positions and linewidths are in cm^{-1}. Predissociation and photoabsorption rate constants are expressed in units of 10^8 s^{-1}.

		$N^+=0$		$N^+=1$		$N^+=2$		
n	$^{11}BH^*$ $k(n)$	E^n	$\Phi\sigma_{AX}(\Delta)$	E^n	$\Phi\sigma_{AX}(\Delta)$	E^n	$\Phi\sigma_{AX}(\Delta)$	$\Gamma_A(n)$
13	5.9	26068.0	0.035	26046.5	0.093	26144.2	0.42	30
14	4.7	26171.6	0.062	26156.0	0.16	26238.4	1.0	24
15	3.8	26254.1	0.14	26241.9	0.31	26329.1	15	20
16	3.2	26310.6	0.27	26314.0	1.1	26391.5	7.4	16
17	2.6	26366.2	2.0	26374.1	18	26443.2	18	13
18	2.2	26412.4	3.4	26422.2	16	26491.0	1.0	11
19	1.9	26451.9	0.32	26463.2	0.92	26528.0	0.38	9.7
20	1.6	26481.7	0.13	26498.2	0.30	26560.3	0.20	8.3
21	1.4	26510.7	0.062	26524.2	0.17	26585.9	0.13	7.2
22	1.2	26535.7	0.036	26551.2	0.098	26610.8	0.087	6.2
23	1.1	26554.7	0.025	26573.2	0.065	26631.2	0.063	5.4
24	0.93	26574.4	0.017	26593.2	0.045	26650.3	0.047	4.8

discussed above, the scan range of ω_3 includes the low-N region of the $A\ ^2\Pi$-$X\ ^2\Sigma^+$ (0,0) band of $^{11}BH^+$ [22], and thus can accommodate $|A\ ^2\Pi\rangle|nl\rangle \leftarrow |X\ ^2\Sigma^+\rangle|nl\rangle$ ICE transitions. From Fig. 1, assuming that ICE conserves n and l, the on-resonance energy $E_A(n,l,N^+,N_A^+)$ of such a transition can be expressed as

$$E_A(n,l,N^+,N_A^+) = T_{AX}(N^+,N_A^+) + V_{\text{ion}}(N^+) - E^n_{N^+} - \frac{R}{(n-\tilde{\mu}_l)^2}. \tag{4}$$

In this equation, the term, $T_{AX}(N^+,N_A^+)$, denotes the rotational line position within the $A^2\Pi$-$X^2\ ^2\Sigma^+$ (0,0) band of $^{11}BH^+$, as given in Table I, $V_{\text{ion}}(N^+)$ represents the rotational ionization thresholds of ^{11}BH for $N^+=0$, 1, and 2, measured from the gateway $B\ ^1\Sigma^+\ \nu'=0$, $N'=0$ state (26 773.6, 26 798.4, and 26 847.8 cm^{-1}, respectively, Ref. [25]), and $E^n_{N^+}$ refers to the experimental energy position of the resonant Rydberg state converging to the specific rotation N^+ of the ground state of the ion (as marked in Fig. 3 and given in Table II). The final term $R/(n-\tilde{\mu}_l)^2$ determines the binding energy of the $|A\ ^2\Pi\rangle|nl\rangle$ Rydberg electron, in terms of, $\tilde{\mu}_l$, an estimated quantum defect, chosen to be 0.9 and 0.5 for ns and np electrons respectively. We assume finite linewidths of $|A\ ^2\Pi\rangle|nl\rangle$ Rydberg features to decrease with n^{-3} as

$$\Gamma_A(n) = \Gamma_{rA}/n^3, \tag{5}$$

where we choose the energy reduced linewidth, Γ_{rA}, as a fitting parameter.

At the resolution of our lasers we can neglect Λ-doubling and spin rotation effects for the $^2\Pi$ and $^2\Sigma^+$ states, respectively. Under such circumstances, angular momentum rules allow one, three, and five pathways for $A\ ^2\Pi \leftarrow X\ ^2\Sigma^+$ valence electron core excitations coming from $N^+=0$, 1, and 2, respectively, as shown in Fig. 5. These are the pathways to which ICE is constrained if optical absorption conserves l.

Importantly, because the photon energy required for any such ICE pathway generally does not exactly match that of the ω_3 resonance populating the $|X\ ^2\Sigma^+\rangle|nl\rangle$ state, sequential absorption does not access the corresponding $|A\ ^2\Pi\rangle|nl\rangle$ state on perfect resonance. The detuning, $\Delta(n,N^+,N_A^+)$, is simply

$$\Delta(n,N^+,N_A^+) = |E^n_{N^+} - E_A(n,N^+,N_A^+)|. \tag{6}$$

We observe an ICE feature if this detuning compares to the linewidth $\Gamma_A(n)$ given by Eq. (5). This detuning can be estimated by comparing the $T_{AX}(N^+,N_A^+)$ transition energy

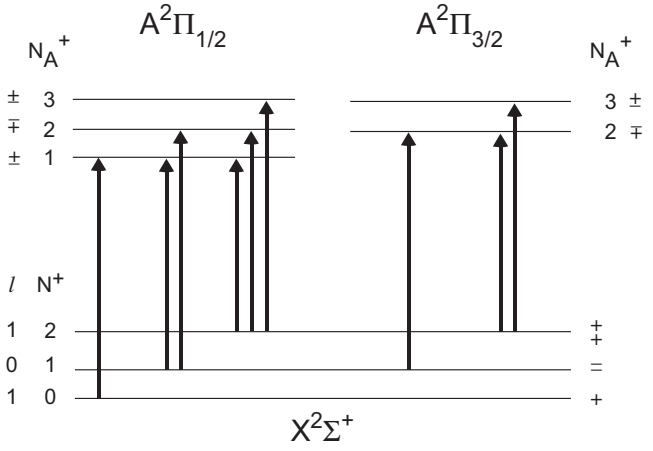

FIG. 5. Nine possible pathways for the $A\ ^2\Pi \leftarrow X\ ^2\Sigma^+$ (0,0) valence electronic promotion of the ion core, based on the three populated levels, $N^+=0$, 1, and 2, of the $X^2\Sigma^+$ ground state (transition energies are listed in Table I).

from Table I with the experimentally observed energy position $E^n_{N^+}$ of the Rydberg resonances. This approximation is equivalent to neglecting the difference in quantum defects for the $|A\ ^2\Pi\rangle|nl\rangle$ and $|X\ ^2\Sigma^+\rangle|nl\rangle$ Rydberg series.

Representing our ω_3 laser pulse by a 10 ns square wave with an energy of 1 mJ, its photon flux Φ in units of photons s^{-1} cm^{-2} varies as

$$\Phi(\omega_3) = 5.7386 \times 10^{29}/\omega_3, \tag{7}$$

for frequency, ω_3 expressed in cm^{-1}.

The photoabsorption rate for an ICE transition is the product $\Phi\sigma_{AX}$, where σ_{AX} is the photoabsorption cross section in cm^2, taken as [31]

$$\sigma_{AX}(n,N^+) = 2.817\ 83 \times 10^{-13} f \sum_p \left(\frac{2}{\Gamma_A(n)}\right) \times \left[1 + \left(\frac{\Delta_p(n,N^+)}{\Gamma_A(n)/2}\right)^2\right]^{-1}. \tag{8}$$

The premultiplicative numerical factor combines fundamental constants $q_e^2/4\pi\epsilon_0 m_e c^2$ in cgs units. The summand p refers to all allowed ICE pathways for a given N^+, as described above. The oscillator strength $f=0.004$ is taken from a theoretical determination of the $A\ ^2\Pi \leftarrow X\ ^2\Sigma^+$ transition moment [32].

The complementary nature of the intensities of features common to the 11 and 12 amu spectra reflects the competition between the processes of light absorption and neutral fragmentation on the part of $|X\ ^2\Sigma^+\rangle|nl\rangle$ $^{11}BH^*$ Rydberg molecules. The observed ratio of signal in mass 12 to that in mass 11 measures concentration of high Rydberg states with excited ion cores, $[^{11}BH^*|A\ ^2\Pi\rangle|nl\rangle]$, to that of $^{11}B^*$ atoms produced by the neutral fragmentation of high Rydberg states built on the cation ground states. This ratio, in turn, reflects the comparative rate of photoabsorption $\Phi\sigma_{AX}$ versus predissociation $k(n)$. Because the 11 amu ion signal requires an additional step of photoionization, only $^{11}B^*$ atoms produced during the 10 ns which the laser fields are still present can contribute. Thus, the intensity of this signal must be scaled using Eq. (2) together with mass balance to determine the total $[^{11}B^*]$, and

$$\frac{[^{11}BH^*|A\ ^2\Pi\rangle|nl\rangle]}{[^{11}B^*]} = \frac{I^n_{12}}{I^n_{11}/(1-e^{-k(n)(10\ \mathrm{ns})})} = \frac{\Phi\sigma_{AX}}{k(n)}, \tag{9}$$

where I^n_{11} and I^n_{12} are the observed intensities in the 11 and 12 amu channels, respectively.

We have determined a measured intensity, I, and linewidth, Γ^n_X, for every Rydberg resonance that appears in the traces recorded for the mass 11 and 12 amu channels. Assuming that the sum of the $^{11}B^+$ and $^{11}BH^+$ ion signal intensity, with the former prescaled as in Eq. (9), is proportional to the population of $^{11}BH^*$ Rydberg molecules generated by the absorption of one quantum of ω_3, we can represent each $|X\ ^2\Sigma^+\rangle|nl\rangle$ Rydberg feature by a Lorentzian line shape as follows:

$$I^n_{N^+}(\omega_3) = [I^n_{11}/(1-e^{-k(n)(10\ \mathrm{ns})}) + I^n_{12}]\left[1 + \left(\frac{\omega_3 - E^n_{N^+}}{\Gamma^n_X}\right)^2\right]^{-1}. \tag{10}$$

By combining Eqs. (9) and (10) and summing over all resonances, we can write the simulated mass 12 signal, $I^{\mathrm{sim}}_{12}(\omega_3)$, as

$$I^{\mathrm{sim}}_{12}(\omega_3) = \sum_{n,N^+} I^n_{N^+}(\omega_3)\left(\frac{k(n)}{\Phi(\omega_3)\sigma_{AX}(n,N^+)} + 1\right)^{-1}. \tag{11}$$

We adjust the energy reduced linewidth, Γ_{rA} in Eq. (5), by least squares in order to fit the pattern of lines in $I^{\mathrm{sim}}_{12}(\omega_3)$ as closely as possible to the observed 12 amu ionization-detected absorption signal shown in Fig. 3(b). The best-fit simulation is given in Fig. 3(c). Table II shows the predissociation constants, $k(n)$, photoabsorption rates, $\Phi\sigma_{AX}$, and finite linewidths of the $|A\ ^2\Pi\rangle|nl\rangle$ features used to produce this simulation. Even though ω_3 transitions to the $|A\ ^2\Pi\rangle|nl\rangle$ Rydberg states generally do not occur on perfect resonance, ICE is nevertheless possible because the detunings in this range do not exceed the linewidths of the $|A\ ^2\Pi\rangle|nl\rangle$ Rydberg resonances, which we assume to be the order of 10 cm^{-1}.

The simulation successfully predicts the ω_3 energy interval over which we observe ICE, and reproduces the intensities of the principal resonances reasonably well with two notable deviations.

$N^+=1$ features with $n=14-21$ appear in the simulation, but are weak in the experimental spectrum. The relatively high core penetration of the *ns* Rydberg electron in this series likely facilitates predissociation of resonantly excited $^{11}BH^*$, thereby quenching the $^{11}BH^+$ photoionization pathway. That these resonances are weak in the $^{11}B^+$ spectrum as well, suggests, perhaps, that Rydberg l regulates the branching ratio in $^{11}BH^*$ predissociation to excited $^{11}B^*$ versus dark, ground state ^{11}B.

The $n=15$, $N^+=2$ $(15p2)$ resonance at 26 329 cm^{-1} also appears in the simulation only. In the $^{11}B^+$ spectrum, this feature forms a complex resonance with a broad interloper, which can be reasonably assigned to a low-n $|A\ ^2\Pi\rangle|nl\rangle$ state. Mixing in this case accelerates the predissociation of the $15p2$ state, diminishing the population available to transfer by ICE.

In addition to the likelihood of specific perturbations, this simulation has some intrinsic limitations that should be mentioned. $|A\ ^2\Pi\rangle|nl\rangle$ autoionizing resonances can be expected to present Lorentzian line shapes for transitions from $|X\ ^2\Sigma^+\rangle|nl\rangle$ originating levels. However, because finite cross sections exist for $\Delta v=+1$ transitions from $|X\ ^2\Sigma^+\rangle|nl\rangle$ levels to vibrational continua underlying these lower lying resonances, they appear with Fano line shapes. Nevertheless, we use Lorentzian line shapes throughout to simplify calculations and limit the number of fitting parameters to one, Γ_{rA}.

We also neglect the effect of varying Hönl-London factors on the photoabsorption cross sections, $\sigma_{AX}(n,N^+)$ for the nine different ICE pathways. Finally, in the absence of experimentally determined values, we estimate the positions of the $|A\ ^2\Pi\rangle|nl\rangle$ features simply by use of average quantum

defects $\tilde{\mu}_l$. Local perturbations are likely to alter these regular line centers, which would alter the expected ICE intensity (see, for example, Ref. [24]). In light of these limitations, our simulation appears to provide a remarkably good approximation of the observed 12 amu spectrum.

V. CONCLUSIONS

By analysis of the multiresonant ionization-detected absorption spectrum of ^{11}BH, we have obtained evidence for the facile electronic excitation of the $^{11}BH^+$ ion core in the presence of a spectator Rydberg electron. Although this phenomenon, known asisolated core excitation (ICE), has been widely exploited as a spectroscopic tool in atoms, this work represents the first observation of ICE in a molecular system.

In our experiments, we observe structure in the $\omega_3 = 26\,100-26\,550$ cm^{-1} region of the predissociation and autoionization spectra of ^{11}BH that reflects the competition between photoabsorption and neutral dissociation. Based on the duration of our laser pulses and on the trends of intensities in the high-n Rydberg states detected through the predissociation channel, we can estimate predissociation rate constants, $k(n)$, and extrapolate them to the region of this competition. Photoabsorption occurs through the $A\,^2\Pi$ -$X^2\Sigma^+$ (0,0) band of $^{11}BH^+$, which lies in the ω_3 scan range. A Rydberg molecule promoted by one quantum of ω_3 to an $|X\,^2\Sigma^+\rangle|nl\rangle$ state has, for some n values, an energy such that a second quantum of ω_3 further excites it to an electronically autoionizing $|A\,^2\Pi\rangle|nl\rangle$ state.

Using a simple mathematical model in which only transitions vertical in n and l are allowed, we show that the interval of n for which the $|A\,^2\Pi\rangle|nl\rangle \leftarrow |X\,^2\Sigma^+\rangle|nl\rangle$ ICE rate exceeds that of dissociation depends on the finite linewidths and positions of $|A\,^2\Pi\rangle|nl\rangle$ features and on the n-dependent predissociative lifetimes of the $|X\,^2\Sigma^+\rangle|nl\rangle$ Rydberg states. We conclude that the initially prepared n-Rydberg electron conserves principal quantum number n and orbital angular momentum l while a strongly allowed $A\,^2\Pi \leftarrow X\,^2\Sigma^+$ valence electronic transition occurs in the ion core.

Building on this work, it seems possible that the introduction of a fourth probe laser could provide a means to determine detailed cross sections for state-to-state ICE transitions in BH from individually selected single $|X\,^2\Sigma^+\rangle|nl\rangle$ states to a full spectrum of accessible $|A\,^2\Pi\rangle|nl\rangle$ autoionizing resonances. Time-resolved pump-probe experiments along these lines could serve well to investigate the evolution of radial Rydberg wave packets near the ion core [33–35].

ACKNOWLEDGMENTS

This work was supported by grants from the U.S. National Science Foundation (CHE-0075833) and the Natural Sciences and Engineering Research Council of Canada (NSERC).

[1] W. E. Cooke, T. F. Gallagher, S. A. Edelstein, and R. M. Hill, Phys. Rev. Lett. **40**, 178 (1978).
[2] L. D. Van Woerkom, J. G. Story, and W. E. Cooke, Phys. Rev. A **34**, 3457 (1986).
[3] J. G. Story, L. D. Van Woerkom, and W. E. Cooke, Phys. Rev. A **34**, 4508 (1986).
[4] R. R. Jones, Phys. Rev. A **58**, 2608 (1998a).
[5] F. Robicheaux, Phys. Rev. A **62**, 033406 (2000).
[6] Y. Zhang, C. J. Dai, and S. B. Li, J. Electron Spectrosc. Relat. Phenom. **148**, 11 (2005).
[7] J. B. M. Warntjes, F. Robicheaux, and L. D. Noordam, Phys. Rev. A **62**, 033407 (2000).
[8] R. R. Jones, B. J. Lyons, M. A. Baig, S. T. Djambova, and T. F. Gallagher, Phys. Rev. A **62**, 033408 (2000).
[9] T. Gallagher, *Rydberg Atoms*, Rydberg Atoms (Cambridge University Press, Cambridge, 1994).
[10] T. P. Softley, Int. Rev. Phys. Chem. **23**, 1 (2004).
[11] J. D. Hofstein, J. G. Goode, and P. M. Johnson, Chem. Phys. Lett. **301**, 121 (1999).
[12] M. C. R. Cockett, Chem. Soc. Rev. **34**, 935 (2005).
[13] K. Muller-Dethlefs and E. W. Schlag, Annu. Rev. Phys. Chem. **42**, 109 (1991).
[14] E. W. Schlag, G. Gerber, S. A. Rice, A. H. Zewail, and M. Shapiro, in *Chemical Reactions and Their Control on the Femtosecond Time Scale 20th Solvay Conference on Chemistry* [Adv. Chem. Phys. **101**, 607 (1997)].
[15] L. C. Zhu and P. Johnson, J. Chem. Phys. **94**, 5769 (1991).
[16] D. P. Taylor, J. G. Goode, J. E. Leclaire, and P. M. Johnson, J. Chem. Phys. **103**, 6293 (1995).
[17] J. G. Goode, J. D. Hofstein, and P. M. Johnson, J. Chem. Phys. **107**, 1703 (1997).
[18] J. G. Goode, J. E. LeClaire, and P. M. Johnson, Int. J. Mass Spectrom. Ion Process. **159**, 49 (1996).
[19] W. Kong, D. Rodgers, and J. Hepburn, Chem. Phys. Lett. **221**, 301 (1994).
[20] W. Jeffers, Chem. Ind. **1961**, 431 (1961).
[21] G. M. Almy and R. B. Horsfall, Jr., Phys. Rev. **51**, 491 (1937).
[22] D. A. Ramsay and P. J. Sarre, J. Chem. Soc., Faraday Trans. 2 **78**, 1331 (1982), part 8.
[23] S. H. Ashworth and J. M. Brown, Technical Report, Rutherford Appleton Laboratory, 1991.
[24] A. T. Gilkison, C. R. Viteri, and E. R. Grant, Phys. Rev. Lett. **92**, 173005 (2004).
[25] C. R. Viteri, A. T. Gilkison, S. J. Rixon, and E. R. Grant, J. Chem. Phys. **124**, 144312 (2006).
[26] A. T. Gilkison, C. R. Viteri, and E. R. Grant, J. Phys.: Conf. Ser. **4**, 261 (2005).
[27] H. Lundberg, Z. S. Li, and P. Jonsson, Phys. Rev. A **63**, 032505 (2001).
[28] R. A. Roig and G. Tondello, J. Phys. B **9**, 2373 (1976).
[29] Y. Zou, T. Brage, and I. Martinson, Adv. Quantum Chem. **70**, 301 (1998).
[30] G. P. Bryant, Y. Jiang, M. Martin, and E. R. Grant, J. Phys. Chem. **96**, 6875 (1992).
[31] R. C. Hilborn, Am. J. Phys. **50**, 982 (1982).
[32] R. Klein, P. Rosmus, and H. J. Werner, J. Chem. Phys. **77**, 3559 (1982).
[33] R. R. Jones, Phys. Rev. A **57**, 446 (1998b).
[34] J. G. Story, D. I. Duncan, and T. F. Gallagher, Phys. Rev. Lett. **71**, 3431 (1993).
[35] M. Strehle, U. Weichmann, and G. Gerber, Phys. Rev. A **58**, 450 (1998).